Geo-Mar Lett (2010) 30:271–281
DOI 10.1007/s00367-009-0171-5

ORIGINAL

Analyses of bottom simulating reflections offshore Arauco and Coyhaique (Chile)

Ivan de la Cruz Vargas Cordero · Umberta Tinivella · Flavio Accaino · Maria Filomena Loreto · Francesco Fanucci · Christian Reichert

Received: 8 January 2009 / Accepted: 19 October 2009 / Published online: 29 October 2009

Abstract Two seismic sections offshore Arauco and Coyhaique, Chile, have been analysed to better define the seismic character of hydrate-bearing sediments. The velocity analysis was used to estimate the gas-phase concentration, which can serve to correlate hydrate presence to the geological features. The velocity model allowed us to recognise the hydrate layer above the bottom simulating reflector (BSR), and the free gas layer below it. The velocity field is affected by strong lateral variation, showing maximum (above the BSR) and minimum (below the BSR) values in the southern sector. Here, highest gas hydrate and free gas concentrations were calculated (15% and 2.7% of total volume respectively). The estimated geothermal gradient ranges from 35 to 95°C/km. In the northern sector, the highest gas hydrate and free gas concentrations are 15% and 0.2% of total volume respectively, and the geothermal gradient is uniform and equal to about 30°C/km.

I. Vargas Cordero (✉) · F. Fanucci
Dipartimento di Scienze Geologiche, Ambientale e Marine,
Università degli Studi di Trieste,
C. San Giovanni, Via E. Weiss 2,
Trieste 34100, Italy
e-mail: ivargas@units.it

I. Vargas Cordero · U. Tinivella · F. Accaino · M. F. Loreto
Istituto Nazionale di Oceanografia e di Geofisica Sperimentale (OGS),
Borgo Grotta 42C,
Trieste, Italy

I. Vargas Cordero
International Centre for Theoretical Physics (ICTP),
Strada Costiera 11,
Trieste, Italy

C. Reichert
Federal Institute for Geosciences and Natural Resources (BGR),
Stilleweg 2,
30655 Hannover, Germany

Introduction

During the last decades, the scientific community has spent considerable effort on studies of gas hydrate in oceanic and permafrost environments. In fact, gas hydrate occurrence has a global significance because of the potential energy resource represented by the large amount of hydrocarbon trapped in the hydrate phase (Milkov 2004). Moreover, gas hydrates may play a role in global climate change (Kvenvolden 1998; Kennett et al. 2003) and geo-hazards, because of drilling and the setting up of seabed installations (Hovland and Gudmestad 2001).

The detection of a bottom simulating reflector (BSR) by using seismic methods has allowed to define the distribution of gas hydrate (e.g. Shipley et al. 1979; Hyndman and Spence 1992; Berndt et al. 2004). The BSR is associated with the interface between overlying sediment containing gas hydrate, which increases compressional seismic velocity, and underlying sediment containing free gas, which decreases compressional seismic velocity (Hyndman and Spence 1992; MacKay et al. 1994). The BSR has been identified in seismic sections in several geological settings, such as in sediments along both convergent and passive margins (Shipley et al. 1979).

Our study area is located along the south central Chile margin on the continental slope between 38 and 45°S (Fig. 1). This area is characterized by the subduction of the Nazca Plate below the South American continental plate. The Nazca Plate is subducting at a rate of about 66 km/million years (Angermann et al. 1999; Kendrick et al.

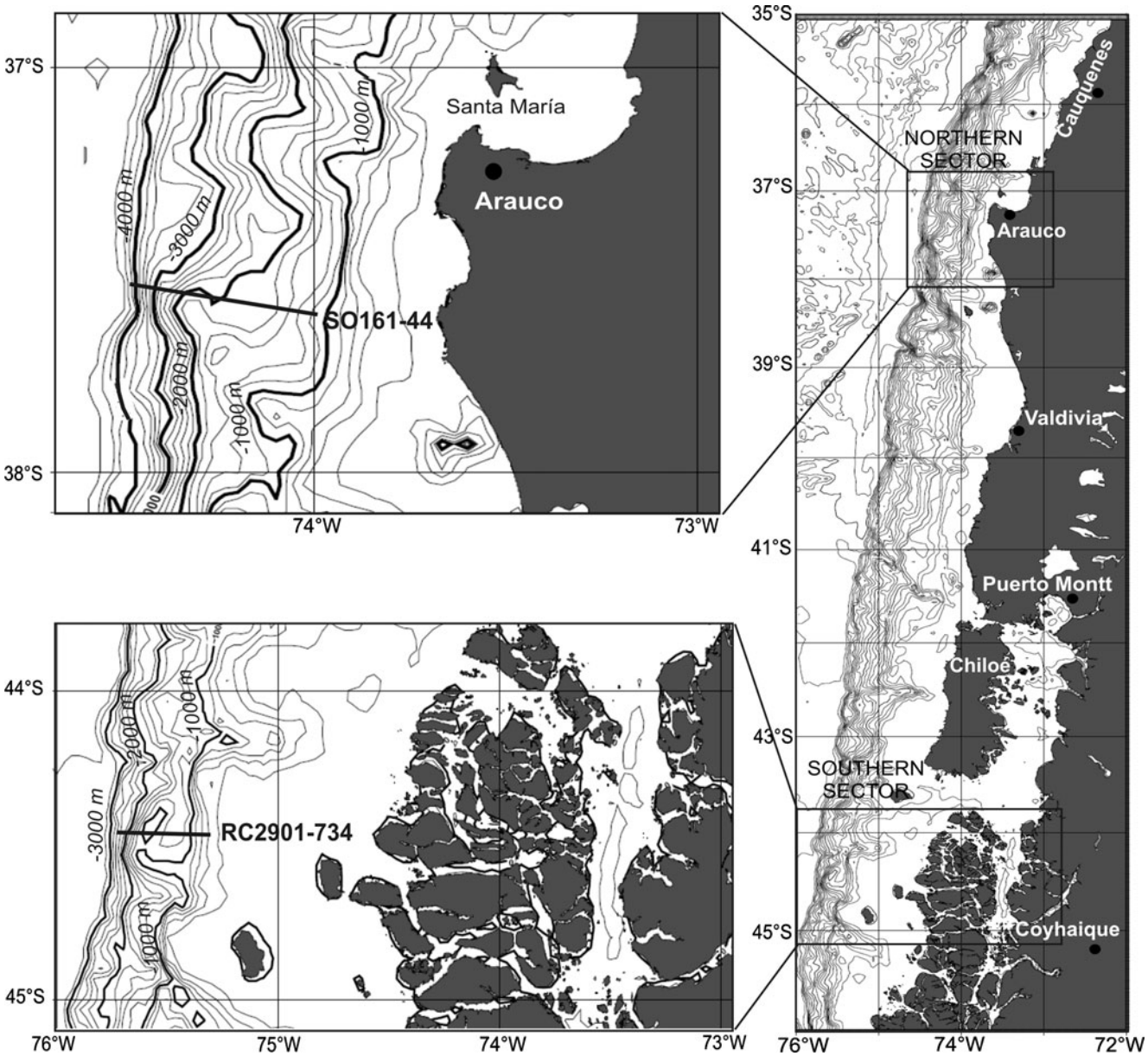

Fig. 1 Location map of the SO161-44 and RC2901-734 seismic lines (*solid lines*). Bathymetry derived by satellite gravimetry (Sandwell and Smith 1997)

2003). High heat flow, associated with the active spreading ridge, has greatly elevated the thermal gradients near the ridge (Bangs and Brown 1995). ODP Leg 141 near the Chilean triple junction furnished an estimate of about 18% and 1% of volume of gas hydrate and free gas concentrations respectively (Brown et al. 1996). In addition, during the Pliocene, an inversion from erosive to accretionary conditions occurred in the fore-arc basin (Melnick and Echtler 2006).

Along the Chilean continental margin, BSRs have been detected these last decades during several geophysical cruises. In particular, a BSR has been recognised along the accretionary prism by several authors (Bangs et al. 1993; Brown et al. 1996; Diaz-Naveas 1999; Morales 2003; Grevemeyer et al. 2003; Vargas Cordero 2009). An important aspect related to gas hydrates is the estimate of gas concentration in the pore space by using seismic data. For this reason, both compressional and shear wave velocities provide information about the presence, distribution and amount of gas hydrate and free gas in marine sediments (Tinivella and Accaino 2000). A quantitative estimate of gas hydrate and free gas concentrations is obtained by fitting the theoretical velocity field with the experimental velocity field (Tinivella 1999; Tinivella et al. 2002). We decided to use a simplified theory, instead of more refined theory (i.e. Carcione and Tinivella 2000;

Chand et al. 2004), because of the lack of direct measurements. In this case, in fact, the main error is due to assumptions of sediment properties.

With the aim of studying gas hydrate along the Chilean continental margin, we analysed two seismic lines, the one located in the northern sector, offshore Arauco, the other in the southern sector offshore Coyhaique (Fig. 1). In fact, our main goal is to map the occurrences of gas hydrates along the Chilean margin and to estimate gas hydrate and free gas concentrations by using seismic data.

The procedure adopted includes (1) determination of the velocity field by using pre-stack depth migration (PSDM), (2) geological interpretation of velocity anomalies and (3) determination of gas hydrate and free gas concentrations by using reference velocity in the absence of gas hydrates and free gas. Then, from sea floor, BSR depths, and sea bottom temperature, the geothermal gradient was estimated. Moreover, to better analyse the seismic properties of the hydrated layer, the instantaneous amplitude was calculated and the values at the BSR were extracted to obtain information about its variability along the margin.

Material and methods

Seismic data

We analysed seismic data acquired by the RV *Sonne* (January–February 2001) within the framework of the project "Subduction Processes off Chile (SPOC)" and by the RV *Conrad* (January–February 1988) within the framework of the project "Mid-Ocean Spreading Ridge (Chile Ridge)" of the Ocean Drilling Program (ODP). We selected the SO161-44 and RC2901-734 seismic lines respectively (Fig. 1).

The SO161-44 seismic line was acquired using a 3,000-m-long digital streamer with 132 channels; from channel 1 to 24 the intertrace was 12.5 m, while from channel 25 to 132 it was 25 m. The seismic source was a tuned array of 20 airguns, providing a total volume of 54.1 l, with a shot spacing of 50 m. The RC2901-734 seismic line was acquired with a 3,000-m-long digital streamer, with 240 channels and an intertrace of 12.5 m. The seismic source was a tuned array of ten airguns with a total volume of 61.3 1, and a shot spacing of 50 m.

Seismic processing was performed by means of the open source Seismic Unix (SU) software (Cohen and Stockwell 2001).

Advanced processing and velocity model building

In order to identify those areas where a detailed velocity analysis would be necessary, we performed standard processing to produce stacked and post-stacked migrated sections (Vargas Cordero 2009). After the identification of the BSR in the post-stacked time migrated sections, we selected a part (about 20 km) of the two lines to perform advanced processing, this being the area where the BSR was strongest and most continuous. The target was to obtain a detailed velocity model by using the PSDM (Kirchhoff algorithm) iteratively and with a layer stripping approach. This method adopts the output of the pre-stack depth migration, the common image gathers (CIGs), to iteratively determine an accurate velocity field (Liu and Bleisten 1995; Yilmaz 2001). To define the initial velocity-depth model, we created a uniformly spaced grid with constant velocity. We used the paraxial ray tracing method to compute the wavefront traveltimes (Beydoun and Keho 1987); the traveltimes in shadow zones are compensated by solving the eikonal equation (Cerveny 1985; Beydoun and Keho 1987). The method that we used to estimate the velocity is based on the analysis of two outputs of the PSDM. Liu and Bleisten (1995) calculated two migration outputs with the same phase, but with different amplitudes. The one uses the original amplitude, the other the small perturbation of the original amplitude. Thus, the ratio of the amplitudes of these two outputs will evaluate the residual velocity. After the PSDM, if the migrated reflections in the CIGs are flat, we can assume that the correct migration velocity to migrate the data is used (Yilmaz 2001). On the contrary, the dip of the reflections in the CIGs indicates error in the migration velocity choice. In this latter case, residual moveout analyses measure the deviations by using the semblance in order to correct the curvatures on the CIGs (Liu and Bleisten 1995).

The energy in the semblance is quantified by the r-parameter, which is a measurement of the flatness deviations of the reflections along the offset. If the r-parameter has a negative value, then it means that the velocity needs to be increased; for a positive value, it needs to be decreased. A zero r-parameter means that the velocity used is correct. To obtain an interval velocity in selected layers, we focused the velocity analysis on selected reflections. At each selected reflection, the updating of the velocity was performed by choosing the r-parameter corresponding to the maximum energy in the semblance, and translating the value of the r-parameter in terms of velocity error at the depth corresponding to the selected reflection depth. The updated velocity model was then used to compute a new migration; the procedure stopped when the energy was well focused around the r-parameter equal to zero for all selected reflections.

We assumed a constant initial velocity equal to 1,480 m/s (water seismic velocity), assuming horizontal and vertical spacing of the grid equal to 10 and 25 m for the SO161-44, and 10 and 12.5 m for the RC2901-734 sections.

Once the first PSDM was performed, we selected the CIG semblance r-parameter corresponding to the sea floor reflection. We reached a satisfactory result after three and five iterations for the SO161-44 and RC2901-734 seismic sections respectively. Then, we started the velocity analysis for a second layer (top: the sea floor; bottom: a horizon between the sea floor and the BSR, hereafter called horizon 1). After 25 and 28 iterations for the two lines respectively, we fixed the velocity for the second layer. A third layer (top: horizon 1; bottom: the BSR) was updated after 40 and 30 iterations for the two lines respectively. Finally, we updated the velocity in the free gas zone, i.e. below the BSR and above a reflection that locally corresponds to the so-called base of free gas reflector (BGR), after 20 and 26 iterations for the two lines respectively. A velocity gradient was included below the BGR and the final velocity models were smoothed before performing the final PSDM; this was because the migration is more stable if the velocity model is smoothed (Liu and Bleisten 1995). Note that the gas hydrate and free gas quantities were estimated using models without smoothening. In order to obtain an accurate image and to attenuate the stretching effects, we produced a stacked section of the CIGs considering the maximum offset of 2,500 m. A trace mixing and band-pass filter were applied to final stacked sections of the CIGs.

In order to check the reliability of our final velocity models, we perturbed the model by ±5% below the sea floor, and performed two new PSDMs for each seismic line. We evaluated the semblances considering these perturbations. Figure 2 shows the semblances of the RC2901-734 seismic line of a selected CIG. Note that the energy is well focused only in the middle panel, suggesting that our velocity model has an error of less than 5%, in agreement with previous studies (Tinivella et al. 2002).

BSR-derived geothermal gradient

It is possible to calculate the geothermal gradient (dT/dZ) by using the following formula:

$$dT/dZ = (T_{BSR} - T_{SEA})/(Z_{BSR} - Z_{SEA})$$

where T_{BSR} and T_{SEA} are the temperatures at the BSR and the sea floor (Grevemeyer et al. 2003) respectively, and Z_{BSR} and Z_{SEA} are the corresponding depths. The BSR and the sea floor depths were obtained from the PSDM sections; the sea floor temperature (equal to 2.2°C) was taken from CTD measurements off Chile from ODP Leg 141 (Grevemeyer and Villinger 2001). The estimate of temperature at the BSR is based on the dissociation temperature-pressure function of gas hydrates (Dickens and Quinby-Hunt 1994; Sloan 1998). We considered two cases: (1) only methane and (2) methane and ethane. In fact, the data indicate that other gases were present, mainly ethane with a saturation of 1% (Froelich et al. 1995). For this reason, we considered a mixture of methane (99%) and ethane (1%).

Estimation of gas hydrates and free gas quantities

The method for estimating gas hydrate and free gas concentrations consists of comparing seismic velocities with theoretical velocity curves in the absence of free gas and gas hydrate, using these as a reference velocity profile. We followed a modified Domenico's approach in order to reproduce the velocity field in the absence of gas, i.e. full

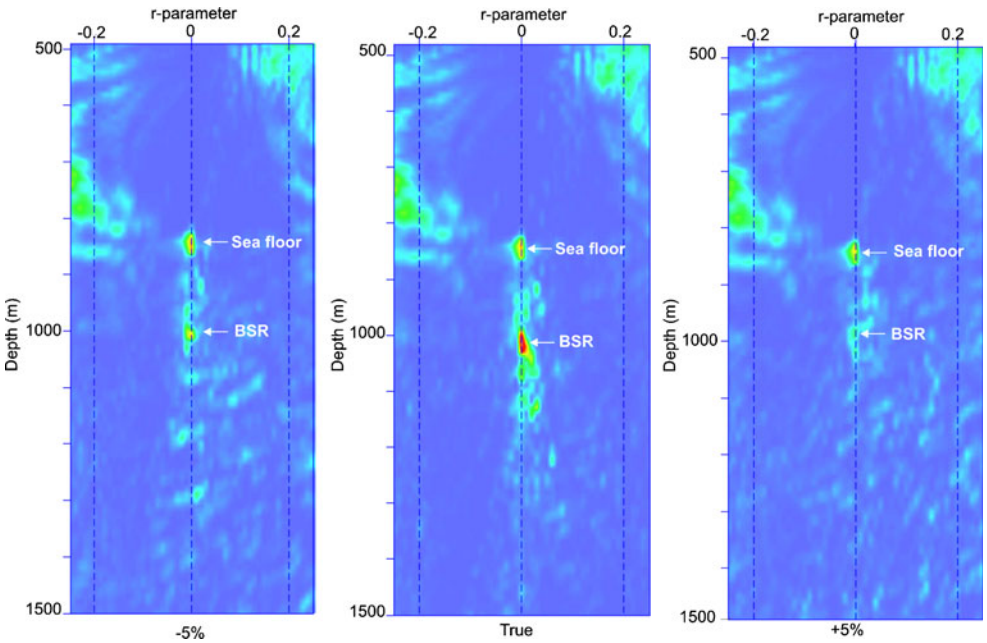

Fig. 2 Semblances of the CIG 42500 obtained performing the PSDM for the RC2901-734 seismic line by using the final velocity model decreased by 5% below sea floor (*left*), the original model (*middle*) and the velocity model increased by 5% below sea floor (*right*). The energies at the sea bottom and the BSR are indicated by *arrows* (see text)

water saturation (Tinivella 1999). A qualitative estimate of concentrations was obtained by comparing the theoretical velocity for full-water saturation to the seismic velocity, evaluated by the PSDM velocity analysis. Positive anomalies indicate the presence of gas hydrates, while negative anomalies indicate the presence of free gas. A quantitative estimate was obtained by fitting the theoretical velocity to the experimental velocity (velocity model obtained by PSDM), increasing the parameters of the theoretical model related to the gas-phase concentrations. The method can model two main distributions to calculate the concentrations of free gas in the pore space: uniform distribution (gas and water in pore space) and patchy distribution (all gas in patches without water). In our case, we considered a uniform distribution of free gas in pore space, because of the low velocity observed in the free gas layer (less than 1,300 m/s; Tinivella 2002). To model the velocity reference curve, we used information regarding the porosity trend available in the literature (Diemer and Forsythe 1995; Grevemeyer and Villinger 2001). In the northern sector, we modelled the reference velocity by fixing the porosity at the sea floor equal to 70%, because of the absence of direct measurements. In the southern sector, we used a variable shallower porosity along the seismic section in order to model the well information (ODP leg 141; Diemer and Forsythe 1995); the shallower porosity is equal to 65% from the beginning of the seismic line until 11,000 m (see Fig. 3), and equal to 50% from 13,000 m to the end of the seismic line. In the middle, we assumed a linear variation of the shallower porosity. The formulas to model the reference porosity are:

$$\Phi_{\text{Northern sector}} = \Phi_i - 0.80z + 0.25z^2$$
$$\Phi_{\text{Southern sector}} = \Phi_i - 0.816z + 0.361z^2$$

where $\Phi_{\text{Northern sector}}$ and $\Phi_{\text{Southern sector}}$ are the reference porosities in the northern and southern sectors respectively, Φ_i is the porosity at the sea floor, and z is the depth below the sea floor in km.

Results

Velocity model, PSDM and instantaneous amplitude sections

The procedure used to perform the PSDM section allowed us to reconstruct the velocity field and to obtain an accurate depth image. In the northern sector (SO161-44), the final velocity model shows a high velocity layer (1,800–2,000 m/s) above the BSR, which can be associated with the presence of gas hydrate. Below the BSR, local low velocities of about 1,550 m/s were detected, associated with the presence of free gas (Fig. 3). In the southern sector (RC2901-734), the high velocity layer associated with the presence of gas hydrate reaches a maximum value of 2,200 m/s, while below the BSR a continuous low velocity layer associated with the presence of free gas reaches a minimum value of 1,250 m/s. A strong lateral velocity variation is evident along the sections. In particular, in the southern sector the hydrate layer shows a minimum value of about 1,700 m/s, which corresponds to a structural high, whereas the maximum value of about 2,200 m/s is present in the fore-arc basin (Fig. 3).

In the northern sector, the PSDM section allowed us to recognise a discontinuous BSR at a depth of 500 mbsf (meter below sea floor), while in the southern sector a strong, continuous and shallower BSR (about 180 mbsf) was recognised. The BGR was identified in both sections, showing a strong continuity only in the southern sector; here, we determined a free gas thickness of about 70 m (Fig. 3). In the southern sector, by contrast, the stratification of the fore-arc basin sediments is mainly parallel to the sea floor and, therefore, it is difficult to recognise the BSR.

The instantaneous amplitude of the BSR varies along the sections and is inversely proportional to the velocity below the BSR, as expected (Fig. 3). Where the BSR is strong and continuous, the instantaneous amplitude shows the highest values, while around faults and fluid escape zones the lowest values are recognised, as confirmed by a less evident BSR (Fig. 3).

BSR-derived geothermal gradient

By using the sea floor and the BSR depths, and knowing the sea bottom temperature (equal to 2.2°C; Grevemeyer and Villinger 2001), we estimated the geothermal gradient. In the northern sector, the geothermal gradient is about 30°C/km. By contrast, in the southern sector a variable geothermal gradient was recognised: the maximum value, equal to 95°C/km, is obtained near the structural high; the minimum value, equal to 35°C/km, is obtained eastwards and westwards (Fig. 4).

Estimation of gas hydrate and free gas quantities

The results of the gas-phase estimates indicate high variability along the sections. Note that in the southern sector the estimate was evaluated considering a variable geothermal gradient (from 35 to 95°C/km) to obtain a more reliable result.

In the northern sector, the highest gas hydrate concentration is located between 9,000 and 13,000 m corresponding to the accretionary wedge (about 15% of total volume; Fig. 5). A similar trend is recognised in the southern sector, where the highest values are located in

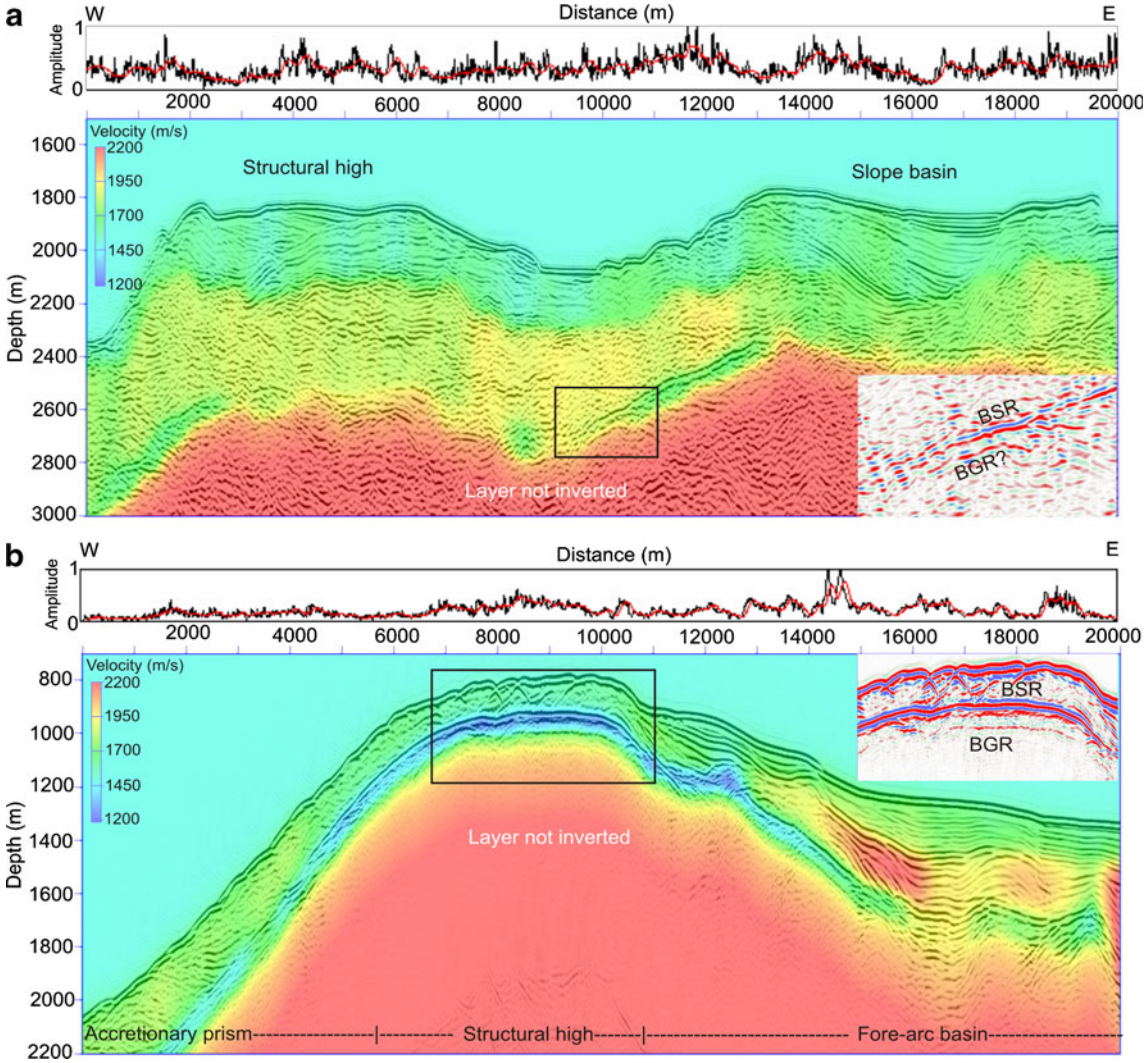

Fig. 3 Final velocity model superimposed on to the pre-stack depth-stack migrated section. *Insert* Detail of the depth section in proximity of the structural high, in which the BSR and the BGR are evident. **a** Northern sector, **b** southern sector. Above each section, the instantaneous amplitude of the BSR is reported and normalized to the maximum value. Vertical exaggeration 1:5

vicinity of the accretionary prism (about 15% of total volume; Fig. 5). On the other hand, the highest free gas concentrations (0.2% of volume) in the northern sector are detected where highest gas hydrate concentrations are present, whereas in the southern sector we observed a free gas distribution with an opposite trend compared to the hydrate distribution. In fact, the highest free gas concentration (2.7%) is located close to the structural high, where the lowest gas hydrate concentration is present. Along this line, towards both sides, the concentration decreases, reaching a value of about 1% (Fig. 5). Finally, in the northern sector we obtained an average of gas hydrate and free gas concentrations equal to 8% and 0.1% respectively, while in the southern sector the average concentrations are equal to 6% and 1% respectively.

Figure 6 shows the modelled porosity along the two seismic sections in which the gas hydrate effect is considered. The reference and seismic velocities are reported at selected distances in order to emphasise the velocity increase/decrease caused by the presence of hydrate/free gas.

Discussion and conclusions

The seismic velocity analysis indicates strong lateral variations in both analysed seismic lines. In the northern sector, we found that the highest and lowest velocities are observed only where the BSR is present (Fig. 3). Note that the reflector selected below the BSR can only be locally associated to the BGR. In the southern sector, above the BSR, the lowest velocity is observed in proximity to the structural high. By contrast, the highest velocity is present in the fore-arc basin. We supposed that in this area the high

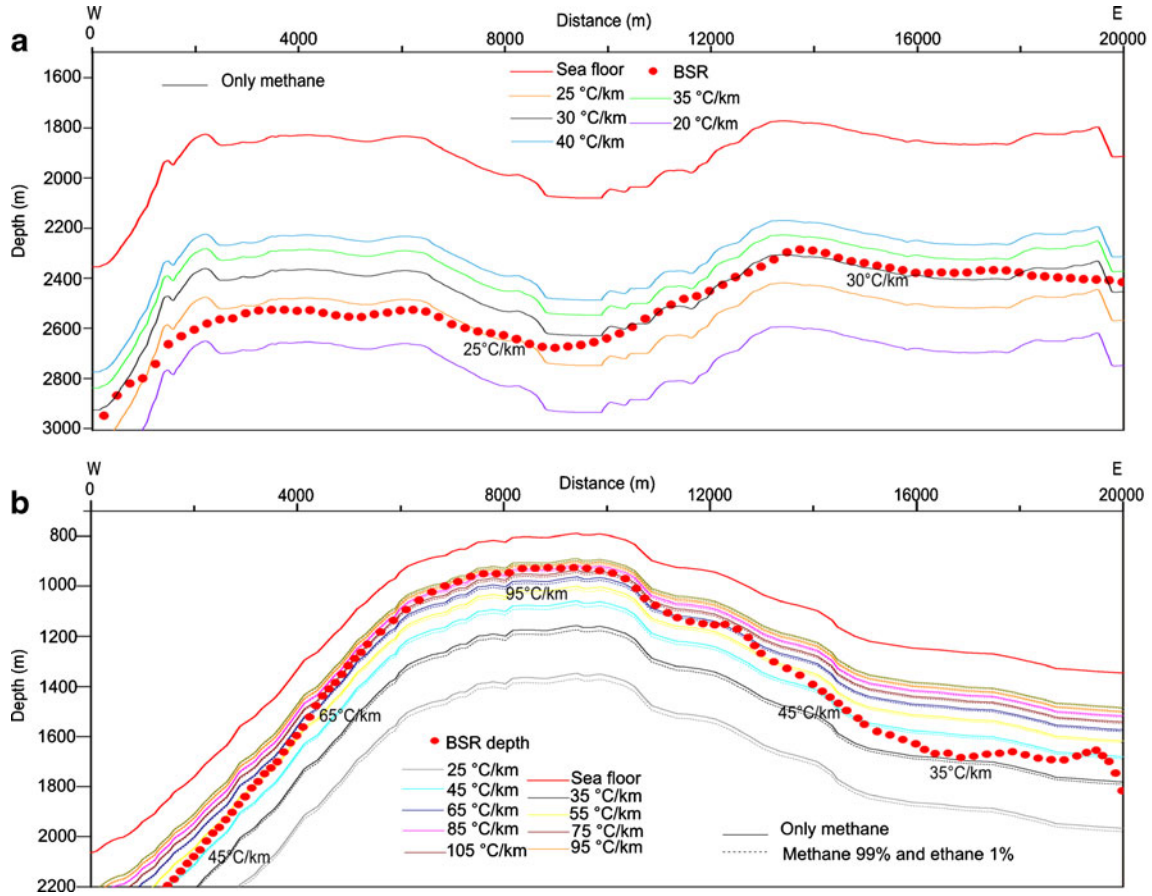

Fig. 4 Theoretical BSR depth evaluated considering diverse geothermal gradients (from 25 to 105°C/km). **a** Northern sector: the *solid lines* refer to the modelling considering hydrate of only methane. **b** Southern sector: the *dashed lines* are evaluated considering a mixture of gases (99% methane and 1% ethane). The sea floor and the BSR depths are indicated by the *red solid line* and *red circles* respectively. Vertical exaggeration 1:5

velocity can be related to two main factors: (1) gas hydrate presence and (2) changes in petro-physical properties related to the different compaction of marine sediments. In fact, continental glaciation effects documented along the southern part of the Chilean margin (Rabassa and Clapperton 1990) may cause porosity reduction and consequent velocity increases. Thus, we supposed that in the southern sector the values that we can estimate for gas hydrate concentration, from seismic velocity, must be significantly decreased. For this reason, in the northern sector, we considered a constant reference velocity, while in the southern sector we assumed a variable reference velocity curve along the section, as explained above, in order to obtain a more realistic estimation of gas hydrate. Below the BSR, we observed an opposite trend: the free gas zone is thicker where the BSR is shallower. Moreover, the lowest velocity observed in proximity of the structural high is in agreement with the hypothesis that it can be considered as a geometrical trap for the accumulation of fluid. Thus, fluid migrates upwards, is transformed into gas hydrate, which in turn reduces permeability and, consequently, allows new fluid to accumulate below it.

We can draw similar conclusions analysing the estimation of the gas-phase concentrations derived by the velocity models. In fact, the high velocity above the BSR means high gas hydrate concentrations (until 15% in both the northern and southern sectors) and the low velocity below the BSR means high free gas concentration (0.2% and 2.7% in the northern and southern sectors respectively). We wish to stress that, in the absence of direct measurements, our estimate is affected by inaccuracy and the main reliable result is the information about the relatively variable distribution of both hydrate and free gas in the pore space along the margin. Nevertheless, our estimation is consistent with the values obtained by other authors analysing different data in the same area (Bangs et al. 1993; Froelich et al. 1995; Brown et al. 1996). For example, Brown et al. (1996) estimated that the gas hydrate concentration ranges from 5 to 20% of volume, while the free gas concentration ranges from 1 to 3% of volume. In any case, our procedure

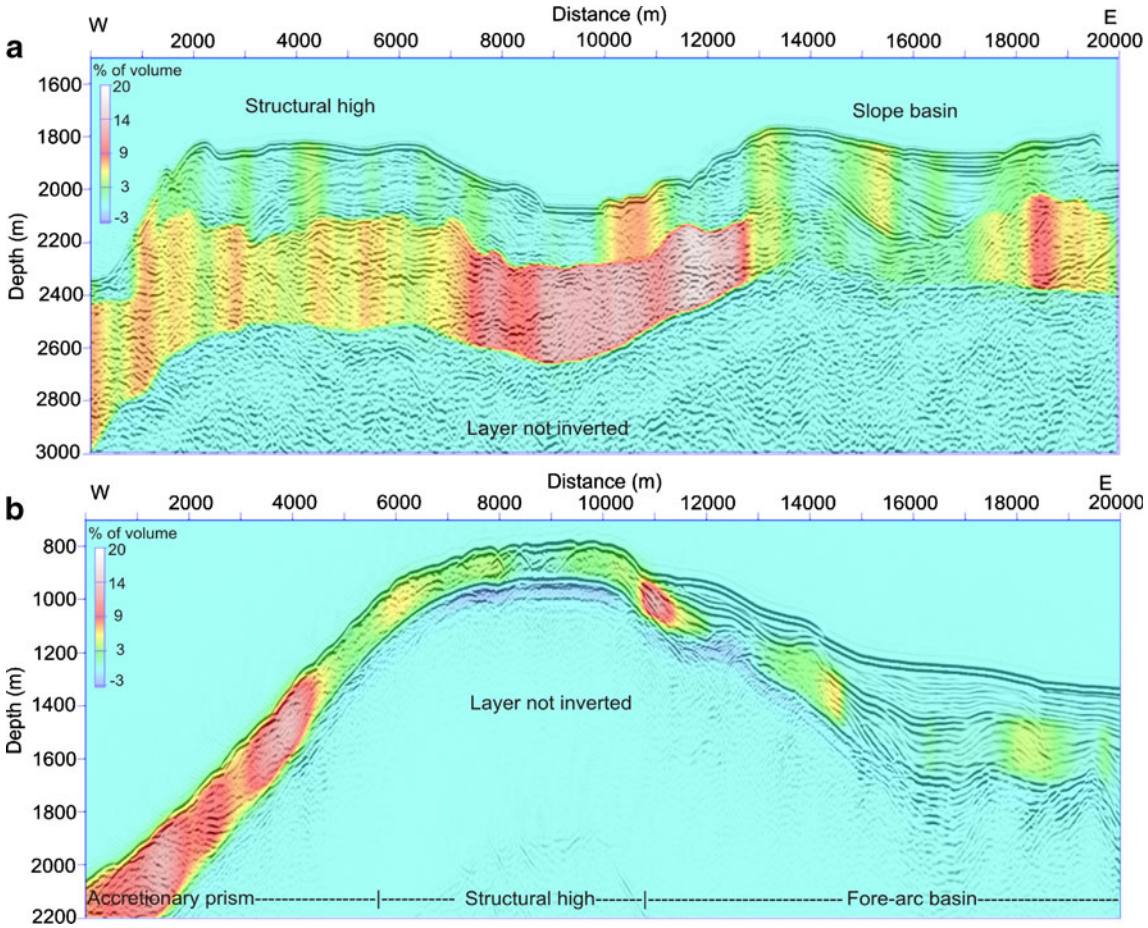

Fig. 5 Concentration models of the gas hydrates (*positive values*) and the free gas (*negative values*) obtained by the velocity models (see text) in **a** the northern and **b** the southern sectors. Vertical exaggeration 1:5

can be used to determine variability at a regional scale, as confirmed by the order of magnitude of our estimate.

The BSR is generally present along the inner part of the accretionary prism. In the northern sector, the BSR is strong and continuous mainly between 9,000 and 13,000 m, becoming discontinuous in the vicinity of structural highs (Fig. 3). In the southern sector, the BSR is present from the middle part of the accretionary prism to the first part of the fore-arc basin. In this part, the BSR disappears possibly due to three main reasons: (1) high sediment compaction, which reduces porosity and the connection between pores (Rabassa and Clapperton 1990); (2) parallel sediment stratification, which masks the presence of the BSR; (3) absence of gas, due to lateral migration towards the structural high.

In the southern sector, the seismic section provides evidence of the presence of a structural high that acts as a structural trap for gas and fluid. The presence of active faults and fluid circulation is also related to the strong variability in BSR depth. In fact, in the southern sector the BSR depth varies from 250 mbsf (in the middle of the accretionary prism) to 130 mbsf (in the structural high), reaching its maximum (330 mbsf) in the fore-arc basin. This depth variability is due partially to the different water depth and partially to the variable geothermal gradient, from 35 to 95°C/km (Fig. 4), caused by fluid migration that affects the gas hydrate stability field. The maximum depth of the BSR, reached in the fore-arc basin, is associated with the decrease of geothermal gradient from 65 to 40°C/km. This strong decrease could be caused by a combination of reduced fluid circulation, increased sedimentation rates, or morphological effect, as can occur along the flank of a structural high (Ruppel 1997; Ganguly et al. 2000). In the northern sector, the BSR depth reaches 500 mbsf. Here, the higher BSR depth (compared to the southern sector) can be explained by the high water depth and by the presence of a lower geothermal gradient (about 30°C/km). It is worth mentioning that our estimated geothermal gradient values are in agreement with published values reported in the literature (Bangs et al. 1993; Brown et al. 1996; Grevemeyer et al. 2003).

As described above, the gas-phase distribution is different in the two sectors. Three main reasons can explain the different trends between the hydrate and free gas

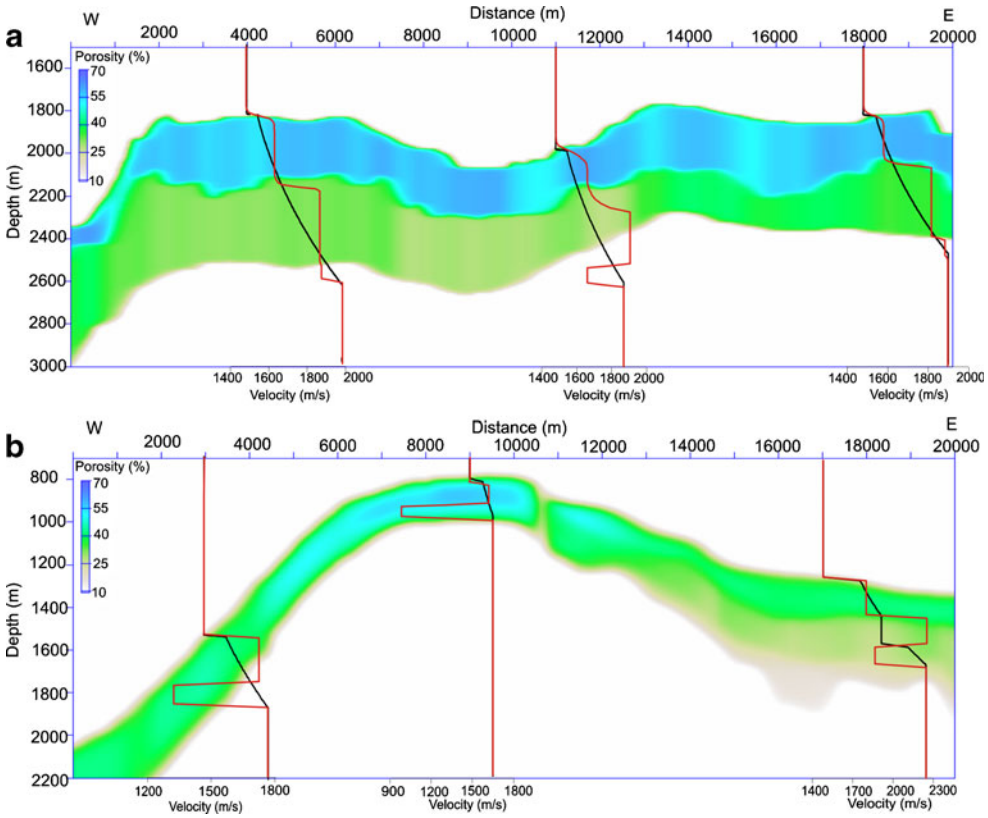

Fig. 6 Effective porosity models with superimposed reference velocity (*black lines*) and seismic velocity (*red lines*) curves for selected points. **a** Northern sector and **b** southern sector. Vertical exaggeration 1:5

concentrations. The first one is related to the possible difference in sediment permeability between the northern (high permeability) and the southern (low permeability) sectors. In fact, high permeability favours hydrate formation in a thick layer. By contrast, low permeability favours gas hydrate formation just at the limit of the stability zone (i.e. BSR) in a thin layer that acts as a sealed layer for free gas accumulation (Klauda and Sandler 2001). Moreover, note that the porosity used to evaluate the reference velocity in the two sectors is in agreement with this hypothesis (highest porosity in the north and lowest porosity in the south).

The second reason is related to a different flux of fluid flow. In the northern sector, we estimated a lowest geothermal gradient, which can be associated with a slow flux and, consequently, a major possibility to form a thick gas hydrate layer. In the southern sector, on the other hand, the estimated high geothermal gradient in proximity of the structural high can be related to a rapid flux that prevents the formation of a thick hydrate layer, which in turn would act as a sealed layer favouring high free gas accumulation below it (Roberts et al. 2006). Finally, it is important to emphasise the different BSR depths in the two sectors (about 2,500 m in the north and about 900 m in the south): from a seismic point of view, this means a different velocity resolution. In fact, the maximum offset (i.e. the maximum velocity depth that can be determined by seismic analysis; Yilmaz 2001) is almost the same in the two cases (about 3,000 m), suggesting that the velocity across the BSR in the southern sector can be better solved than is the case with the northern sector. Maybe, all these points can contribute to explain the different relationships between hydrate and free gas distributions along the Chilean margin.

In conclusion, our study suggests that gas hydrate can play an important role in this part of the Chilean margin, for two main reasons. The first one is related to gas hydrate as a potential resource. In fact, the local high concentrations of both hydrate and free gas suggested by previous studies and the present study could be considered as future energy resources. The second reason is related to geo-hazards due to intense seismicity affecting the region (Grevemeyer et al. 2006; Lange 2008). A possible strong earthquake could generate anomalous sea waves, which represent important geo-hazards for human activities in the coastal zone. On the other hand, an earthquake can destabilise hydrates, amplifying the geo-hazard phenomena, as evidenced by several authors (cf. Mienert et al. 2005). Moreover, the high amount of free gas, presumably in overpressure condition and present in vicinity of the structural high in the southern sector, could be naturally released and trigger submarine slides towards the sides of the structural high, inducing hydrate instability. These scenarios should be taken into account in environmental studies in this part of the Chilean margin.

Acknowledgments The authors are very grateful to Joyce Alsop and Volkmar Damm for seismic data provided by the Lamont Doherty Earth Laboratory (LDEO), USA and the Federal Institute for Geosciences and Natural Resources (BGR), Germany respectively. We thank Ernest Ohene Asare and Frank Calixto Mory for useful English revision. This work was partially supported by The International Centre for Theoretical Physics (Trieste).

References

Angermann D, Klotz J, Reiberg C (1999) Space-geodetic estimation of the Nazca-South American Euler vector. Earth Planet Sci Lett 171:329–334

Bangs NL, Brown KM (1995) Regional heat flow in the vicinity of the Chile Triple Junction constrained by the depth of the bottom simulating reflector. In: Lewis SD, Behrmann JH, Musgrave RJ et al (eds) Proc ODP Scientific Results 141:253–258

Bangs NL, Sawyer DS, Golovchenko X (1993) Free gas at the base of the gas hydrate zone in the vicinity of the Chile triple Junction. Geology 21:905–908

Berndt C, Bunz S, Clayton T, Mienert J, Saunders M (2004) Seismic character of bottom-simulating-reflectors: examples from the mid Norwegian margin. Mar Pet Geol 21:723–733

Beydoun WB, Keho TH (1987) The paraxial ray method. Geophysics 52:1639–1653

Brown KM, Bangs NL, Froelich PN, Kvenvolden KA (1996) The nature, distribution, and origin of gas hydrate in the Chile Triple Junction region. Earth Planet Sci Lett 139:471–483

Carcione JM, Tinivella U (2000) Bottom simulating reflectors: seismic velocities and AVO effects. Geophysics 65:54–67

Cerveny V (1985) Ray synthetic seismograms for complex two-dimensional and three-dimensional structures. J Geophys 58:2–26

Chand S, Minshull TA, Gei D, Carcione JM (2004) Elastic velocity models for gas-hydrate-bearing sediments—a comparison. Geophys J Int 159:573–590

Cohen JK, Stockwell JW (2001) CWP/SU: seismic unix release 35: a free package for seismic research and processing. Center for Wave Phenomena, Colorado School of Mines, Golden

Diaz-Naveas J (1999) Sediment subduction and accretion at the Chilean convergent margin between 35' and 40'S. Dissertation, University of Kiel, Kiel

Dickens GR, Quinby-Hunt MS (1994) Methane hydrate stability in seawater. Geophys Res Lett 21:2115–2118

Diemer JA, Forsythe R (1995) Grain size variations within slope facies recovered from the Chile Margin Triple Junction. In: Lewis SD, Behrmann JH, Musgrave RJ et al (eds) Proc ODP Scientific Results 141:79–94

Froelich PN, Kvenvolden KA, Torres ME, Waseda A, Didyk BM Lorenson TD (1995) Geochemical evidence for gas hydrate in sediment near the Chile triple junction. In: Lewis SD, Behrmann JH, Musgrave RJ et al (eds) Proc ODP Scientific Results 141:279–286

Ganguly N, Spence GD, Chapman NR, Hyndman RD (2000) Heat flow variations from bottom simulating reflectors on the Cascadia margin. Mar Geol 164:53–68

Grevemeyer I, Villinger H (2001) Gas hydrate stability and the assessment of heat flow through continental margins. Geophys J Int 145:647–660

Grevemeyer I, Diaz-Naveaz JL, Ranero CR, Villenger HW, Party Ocean Drilling Program Scientific (2003) Heat flow over the decensing Nazca plate in Central Chile, 32°S to 41°S: observations from ODP Leg 202 and the occurrence of natural gas hydrates. Earth Planet Sci Lett 213:285–298

Grevemeyer I, Kaul N, Díaz-Naveas JL (2006) Geothermal evidence for fluid flow through the gas hydrate stability field off Central Chile-transient flow related to large subduction zone earthquakes? Geophys J Int 166:461–468

Hovland M, Gudmestad OT (2001) Potential influence of gas hydrates on seabed installations. In: Paull CK, Dillon WP (eds) Natural gas hydrates: occurrence, distribution and detection. Geophys Monogr Am Geophys Union 124:307–315

Hyndman RD, Spence GD (1992) A seismic study of methane hydrate marine bottom-simulating-reflectors. J Geophys Res 97:6683–6698

Kendrick E, Bevis M, Smalley R, Brooks B, Vargas RC, Lauría E, Fortes LPS (2003) The Nazca-South America Euler vector and its rate of change. J S Am Earth Sci 16:125–131

Kennett JP, Cannariato KG, Hendy IL, Behl RJ (2003) Methane hydrates in Quaternary climate change: the clathrate gun hypothesis. American Geophysical Union, Washington

Klauda JB, Sandler SI (2001) Modeling gas hydrate phase equilibria in laboratory and natural porous media. Industrial Eng Chem Res 40:4197–4208

Kvenvolden KA (1998) A primer on the geological occurrence of gas hydrate. In: Henriet JP, Mienert J (eds) Gas hydrates: relevance to world margin stability and climate change. Geological Society, London, pp 9–30

Lange D (2008) The South Chilean subduction zone between 41° and 43.5°S: seismicity, structure and state of stress. Dissertation, University of Potsdam, Potsdam

Liu Z, Bleisten N (1995) Migration velocity analysis: theory and an iterative algorithm. Geophysics 60:142–153

MacKay ME, Jarrard RD, Westbrook GK, Hyndman RD (1994) Origin of bottom-simulating reflectors: geophysical evidence from the Cascadia accretionary prism. Geology 22:459–462

Melnick D, Echtler HP (2006) Inversion of forearc basins in south-central Chile caused by rapid glacial age trench fill. Geology 34:709–712

Mienert J, Vanneste M, Bünz S, Andreassen K, Haflidasson H, Sejrup HP (2005) Ocean warming and gas hydrate stability on the mid-Norwegian margin at Storegga Slide. Mar Pet Geol 2:233–244

Milkov AV (2004) Global estimates of hydrate-bound gas in marine sediments: how much is really out there? Earth-Sci Rev 66:183–197

Morales E (2003) Methane hydrates in the Chilean continental margin. J Biotechnol. http://ejb.ucv.cl/content/vol6/issue2/issues/1/

Rabassa J, Clapperton C (1990) Quaternary glaciations of the Southern Andes, Quaternary glaciations in the Southern Hemisphere. Quat Sci Rev 9:153–174

Roberts HH, Hardage BA, Shedd WW, Hunt J Jr (2006) Seafloor reflectivity—an important seismic property for interpreting fluid/gas expulsion geology and the presence of gas hydrate. Leading Edge 25:620–628

Ruppel C (1997) Anomalously cold temperatures observed at the base of the gas hydrate stability zone on the US passive margin. Geology 25:699–702

Sandwell DT, Smith WHF (1997) Marine gravity anomaly from Geosat and ERS-1 satellite altimetry. J Geophys Res 102:10039–10054

Shipley TH, Houston MH, Buffler RT, Shaub FJ, McMillen KJ, Ladd JW, Worzel JL (1979) Seismic reflection evidence for the widespread occurrence of possible gas hydrate horizons on continental slopes and rises. AAPG Bull 63:2204–2213

Sloan ED (1998) Clathrate hydrates of natural gases. Marcel Dekker, New York

Tinivella U (1999) A method for estimating gas hydrate and free gas concentrations in marine sediments. Boll Geofis Teorica Applicata 40:19–30

Tinivella U (2002) The seismic response to overpressure versus gas hydrate and free gas concentration. J Seismic Explor 11:283–305

Tinivella U, Accaino F (2000) Compressional velocity structure and Poisson's ratio in marine sediments with gas hydrate and free gas by inversion of reflected and refracted seismic data (South Shetland Islands, Antarctica). Mar Geol 164:13–27

Tinivella U, Accaino F, Camerlenghi A (2002) Gas hydrate and free gas distribution from inversion of seismic data on the South Shetland margin (Antarctica). Mar Geophys Res 23:109–123

Vargas Cordero I (2009) Gas hydrate occurrence and morpho-structures along Chilean margin. Dissertation, University of Trieste, Trieste

Yilmaz O (2001) Seismic data analysis: processing, inversion and interpretation of seismic data. Society of Exploration Geophysicists, Tulsa